

COMPARISON OF HECTOSPEC VIRIAL MASSES WITH SZE MEASUREMENTS

KENNETH RINES^{1,2}, MARGARET J. GELLER², AND ANTONALDO DIAFERIO^{3,4}

Draft version May 5, 2010

ABSTRACT

We present the first comparison of virial masses of galaxy clusters with their Sunyaev-Zel'dovich Effect (SZE) signals. We study 15 clusters from the Hectospec Cluster Survey (HeCS) with MMT/Hectospec spectroscopy and published SZE signals. We measure virial masses of these clusters from an average of 90 member redshifts inside the radius r_{100} . The virial masses of the clusters are strongly correlated with their SZE signals (at the 99% confidence level using a Spearman rank-sum test). This correlation suggests that Y_{SZ} can be used as a measure of virial mass. Simulations predict a powerlaw scaling of $Y_{SZ} \propto M_{200}^\alpha$ with $\alpha \approx 1.6$. Observationally, we find $\alpha = 1.11 \pm 0.16$, significantly shallower (given the formal uncertainty) than the theoretical prediction. However, the selection function of our sample is unknown and a bias against less massive clusters cannot be excluded (such a selection bias could artificially flatten the slope). Moreover, our sample indicates that the relation between velocity dispersion (or virial mass estimate) and SZE signal has significant intrinsic scatter, comparable to the range of our current sample. More detailed studies of scaling relations are therefore needed to derive a robust determination of the relation between cluster mass and SZE.

Subject headings: galaxies: clusters: individual — galaxies: kinematics and dynamics — cosmology: observations

1. INTRODUCTION

Clusters of galaxies are the most massive virialized systems in the universe. The normalization and evolution of the cluster mass function is therefore a sensitive probe of the growth of structure and thus cosmology (e.g., Rines et al. 2007, 2008; Vikhlinin et al. 2009; Henry et al. 2009; Mantz et al. 2008; Rozo et al. 2008, and references therein). Many methods exist to estimate cluster masses, including dynamical masses from either galaxies (Zwicky 1937) or intracluster gas (e.g., Fabricant et al. 1980), gravitational lensing (e.g., Smith et al. 2005; Richard et al. 2010), and the Sunyaev-Zel'dovich effect (SZE Sunyaev & Zeldovich 1972). In practice, these estimates are often made using simple observables, such as velocity dispersion for galaxy dynamics or X-ray temperature for the intracluster gas. If one of these observable properties of clusters has a well-defined relation to the cluster mass, a large survey can yield tight constraints on cosmological parameters (e.g., Majumdar & Mohr 2004). There is thus much interest in identifying cluster observables that exhibit tight scaling relations with mass (Kravtsov et al. 2006; Rozo et al. 2008). Numerical simulations indicate that X-ray gas observables (Nagai et al. 2007) and SZE signals (Motl et al. 2005) are both candidates for tight scaling relations. Both methods are beginning to gain observational support (e.g., Henry et al. 2009; Lopes et al. 2009; Mantz et al. 2009; Locutus Huang et al. 2009). Dynamical masses from galaxy velocities are unbiased

in numerical simulations (Diaferio 1999; Evrard et al. 2008), and recent results from hydrodynamical simulations indicate that virial masses may have scatter as small as $\sim 5\%$ (Lau et al. 2010).

Previous studies have compared SZE signals to hydrostatic X-ray masses (Bonamente et al. 2008; Plagge et al. 2010) and gravitational lensing masses (Marrone et al. 2009, hereafter M09). Here, we make the first comparison between virial masses of galaxy clusters and their SZE signals. We use SZE measurements from the literature and newly-measured virial masses of 15 clusters from extensive MMT/Hectospec spectroscopy. This comparison tests the robustness of the SZE as a proxy for cluster mass and the physical relationship between the SZE signal and cluster mass. Large SZ cluster surveys are underway and are beginning to yield cosmological constraints (Carlstrom et al. 2010; Hincks et al. 2010; Staniszewski et al. 2009).

We assume a cosmology of $\Omega_m=0.3$, $\Omega_\Lambda=0.7$, and $H_0=70 \text{ km s}^{-1} \text{ Mpc}^{-1}$ for all calculations.

2. OBSERVATIONS

2.1. Optical Photometry and Spectroscopy

We are completing the Hectospec Cluster Survey (HeCS), a study of an X-ray flux-limited sample of 53 galaxy clusters at moderate redshift with extensive spectroscopy from MMT/Hectospec. HeCS includes all clusters with ROSAT X-ray fluxes of $f_X > 5 \times 10^{-12} \text{ erg s}^{-1}$ at $[0.5-2.0]\text{keV}$ from the Bright Cluster Survey (BCS Ebeling et al. 1998) or REFLEX survey (Böhringer et al. 2004) with optical imaging in the Sixth Data Release (DR6) of SDSS (Adelman-McCarthy et al. 2008). We use DR6 photometry to select Hectospec targets. The HeCS targets are all brighter than $r=20.8$ (SDSS catalogs are 95% complete for point sources to $r \approx 22.2$). Out of the HeCS sample, 15 clusters have published SZ measurements.

kenneth.rines@wwu.edu

¹ Department of Physics & Astronomy, Western Washington University, Bellingham, WA 98225; kenneth.rines@wwu.edu

² Smithsonian Astrophysical Observatory, 60 Garden St, Cambridge, MA 02138

³ Università degli Studi di Torino, Dipartimento di Fisica Generale “Amedeo Avogadro”, Torino, Italy

⁴ Istituto Nazionale di Fisica Nucleare (INFN), Sezione di Torino, Torino, Italy

2.1.1. Spectroscopy: MMT/Hectospec and SDSS

HeCS is a spectroscopic survey of clusters in the redshift range $0.10 \leq z \leq 0.30$. We measure spectra with the Hectospec instrument (Fabricant et al. 2005) on the MMT 6.5m telescope. Hectospec provides simultaneous spectroscopy of up to 300 objects across a diameter of 1° . This telescope and instrument combination is ideal for studying the virial regions and outskirts of clusters at these redshifts. We use the red sequence to preselect likely cluster members as primary targets, and we fill fibers with bluer targets (Rines et al. in prep. describes the details of target selection). We eliminate all targets with existing SDSS spectroscopy from our target lists but include these in our final redshift catalogs.

Of the 15 clusters studied here, one was observed with a single Hectospec pointing and the remaining 14 were observed with two pointings. Using multiple pointings and incorporating SDSS redshifts of brighter objects mitigate fiber collision issues. Because the galaxy targets are relatively bright ($r \leq 20.8$), the spectra were obtained with relatively short exposure times of 3×600 s to 4×900 s under a variety of observing conditions.

Figure 1 shows the redshifts of galaxies versus their projected clustocentric radii for the 15 clusters studied here. The infall patterns are clearly present in all clusters. We use the caustic technique (Diaferio 1999) to determine cluster membership. Briefly, the caustic technique uses a redshift-radius diagram to isolate cluster members in phase space by using an adaptive kernel estimator to smooth out the galaxies in phase space, and then determining the edges of this distribution (see Diaferio 2009, for a recent review). This technique has been successfully applied to optical studies of X-ray clusters, and yields cluster mass estimates in agreement with estimates from X-ray observations and gravitational lensing (e.g., Rines et al. 2003; Biviano & Girardi 2003; Diaferio et al. 2005; Rines & Diaferio 2006; Rines et al. 2007, and references therein).

We apply the prescription of Danese et al. (1980) to determine the mean redshift cz_\odot and projected velocity dispersion σ_p of each cluster from all galaxies within the caustics. We calculate σ_p using only the cluster members projected within r_{100} estimated from the caustic mass profile.

2.2. SZE Measurements

The SZE detections are primarily from Bonamente et al. (2008, hereafter B08), supplemented by three measurements from Marrone et al. (2009, hereafter M09). Most of the SZ data were obtained with the OVRO/BIMA arrays; the additional clusters from M09 were observed with the Sunyaev-Zel'dovich Array (SZA; e.g., Muchovej et al. 2007).

Numerical simulations indicate that the integrated Compton y-parameter Y_{SZ} has smaller scatter than the peak y-decrement y_{peak} (Motl et al. 2005), so B08 and M09 report only Y_{SZ} . Although y_{peak} should be nearly independent of redshift, Y_{SZ} depends on the angular size of the cluster. The quantity $Y_{SZ}D_A^2$ removes this dependence. Thus, we compare our dynamical mass estimates to this quantity rather than y_{peak} or Y_{SZ} . Table 1 summarizes the SZ data and optical spectroscopy.

It is also critical to determine the radius within which

Y_{SZ} is determined. B08 use r_{2500} , the radius that encloses an average density of 2500 times the critical density at the cluster's redshift; r_{2500} has physical values of 300–700 kpc for the massive clusters studied by B08 (470–670 kpc for the subsample studied here). M09 use a physical radius of 350 kpc because this radius best matches their lensing data.

To use both sets of data, we must estimate the conversion between $Y_{SZ}(r_{2500})$ measured within r_{2500} and $Y_{SZ}(r = 350 \text{ kpc})$ measured within the smaller radius $r = 350 \text{ kpc}$. There are 8 clusters analyzed in both B08 and M09 (5 of which are in HeCS). We perform a least-squares fit to $Y_{SZ}(r_{2500}) - Y_{SZ}(r = 350 \text{ kpc})$ to determine an approximate aperture correction for the M09 clusters. We list both quantities in Table 1.

3. RESULTS

We examine two issues: (1) the strength of the correlation between SZE signal and the dynamical mass and (2) the slope of the relationship between them. Figure 2 shows the $Y_{SZ} - \sigma_p$ relation. Here, we compute σ_p for all galaxies inside both the caustics and the radius $r_{100,c}$ defined by the caustic mass profile [r_δ is the radius within which the enclosed density is δ times the critical density $\rho_c(z)$].

Because we make the first comparison of dynamical properties and SZE signals, we first confirm that these two variables are well correlated. A nonparametric Spearman rank-sum test (one-tailed) rejects the hypothesis of uncorrelated data at the 98.4% confidence level. The strong correlation in the data suggests that both σ_p and $Y_{SZ}D_A^2$ increase with increasing cluster mass.

Hydrodynamic numerical simulations indicate that Y_{SZ} (integrated to r_{500}) scales with cluster mass as $Y_{SZ} \propto M_{500}^\alpha$, where $\alpha=1.60$ with radiative cooling and star formation, and 1.61 for simulations with radiative cooling, star formation, and AGN feedback ($\alpha=1.70$ for non-radiative simulations, Motl et al. 2005). Combining this result with the virial scaling relation of dark matter particles, $\sigma_p \propto M_{200}^{0.336 \pm 0.003}$ (Evrard et al. 2008), the expected scaling is $Y_{SZ} \propto \sigma_p^{4.76}$ (we assume that $M_{100} \propto M_{500}$). The right panels of Figure 2 shows this predicted slope (dashed lines).

The bisector of the least-squares fits to the data has a slope of 2.94 ± 0.74 , significantly shallower than the predicted slope of 4.8.

We recompute the velocity dispersions $\sigma_{p,A}$ for all galaxies within one Abell radius (2.14 Mpc) and inside the caustics. Surprisingly, the correlation is slightly stronger (99.4% confidence level). This result supports the idea that velocity dispersions computed within a fixed physical radius retain strong correlations with other cluster observables, even though we measure the velocity dispersion inside different fractions of the virial radius for clusters of different masses. Because cluster velocity dispersions decline with radius (e.g. Rines et al. 2003; Rines & Diaferio 2006), $\sigma_{p,A}$ may be smaller than $\sigma_{p,100}$ (measured within $r_{100,c}$) for low-mass clusters, perhaps exaggerating the difference in measured velocity dispersions relative to the differences in virial mass (i.e., $\sigma_{p,A}$ of a low-mass cluster may be measured within $2r_{100}$ while $\sigma_{p,A}$ of a high-mass cluster may be measured within r_{100} ; the ratio $\sigma_{p,A}$ of these clusters would be exaggerated rel-

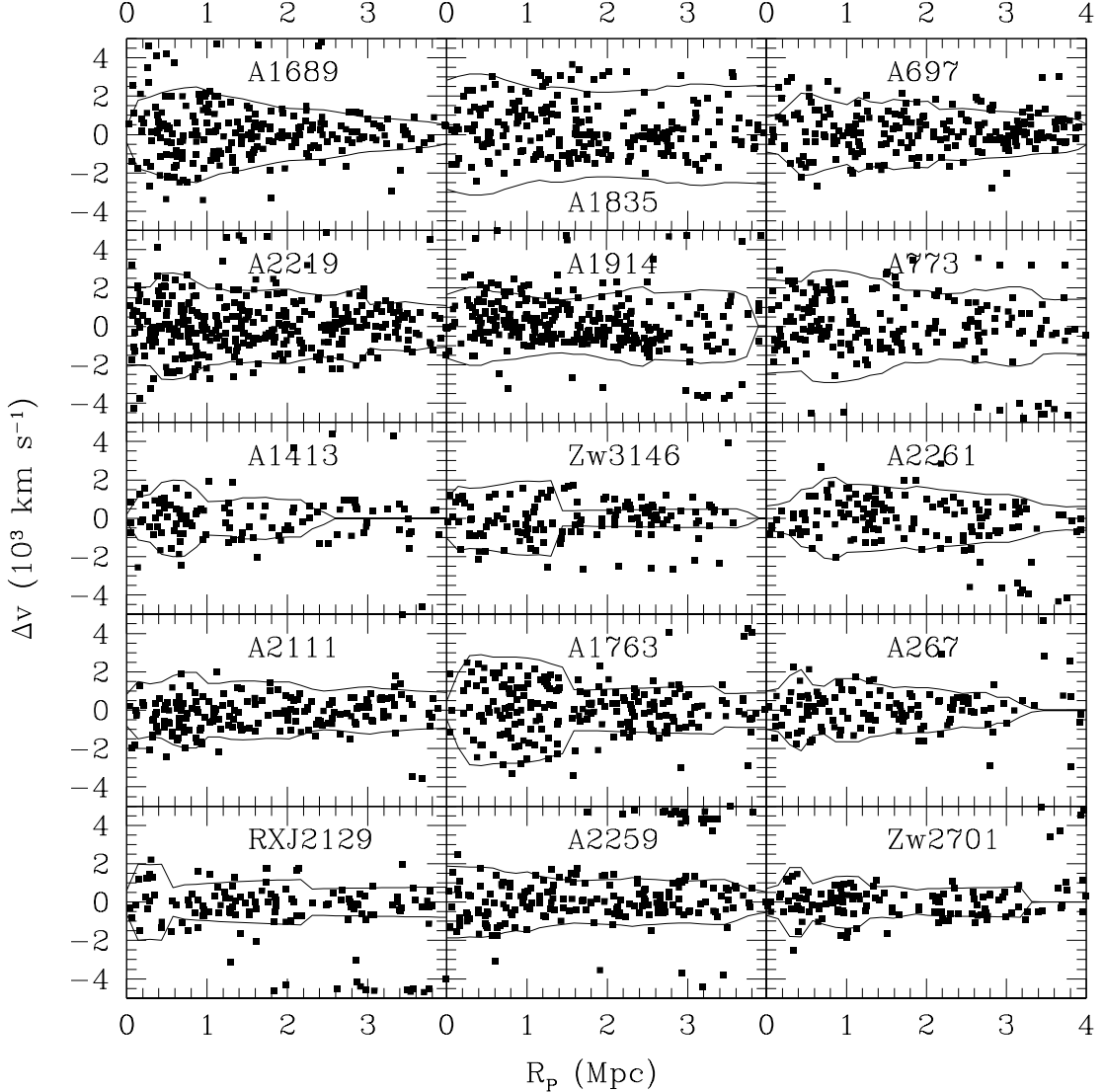


FIG. 1.— Redshift versus projected clustocentric radius for the 15 HeCS clusters studied here. Clusters are ordered left-to-right and top-to-bottom by decreasing values of $Y_{\text{SZ}} D_A^2(r_{2500})$. The solid lines show the locations of the caustics, which we use to identify cluster members. The Hectospec data extend out to ~ 8 Mpc; the figure shows only the inner 4 Mpc to focus on the virial regions.

ative to the ratio $\sigma_{p,100}$). Future cluster surveys with enough redshifts to estimate velocity dispersions but too few to perform a caustic analysis should still be sufficient for analyzing scaling relations.

Because of random errors in the mass estimation, the virial mass and the caustic mass within a given radius do not necessarily coincide. Therefore, the radius r_{100} depends on the mass estimator used. Figure 2 shows the scaling relations for two estimated masses $M_{100,c}$ and $M_{100,v}$; $M_{100,c}$ is the mass estimated within $r_{100,c}$ (where both quantities are defined from the caustic mass profile), and $M_{100,v}$ is the mass estimated within $r_{100,v}$ (both quantities are estimated with the virial theorem, e.g., Rines & Diaferio 2006). including galaxies projected inside $r_{100,v}$. Similar to σ_p , there is a clear correlation between $M_{100,v}$ and $Y_{\text{SZ}} D_A^2$ (99.0% confidence with a Spearman test). The strong correlation of dynamical mass with SZE also holds for $M_{100,c}$ estimated directly

from the caustic technique (99.8% confidence).

The bisector of the least-squares fits has a slope of 1.11 ± 0.16 , again significantly shallower than the predicted slope of 1.6. This discrepancy has two distinct origins. By looking at the distribution of the SZE signals in Figure 2, we see that, at a given velocity dispersion or mass, the SZE signals have a scatter which is a factor of ~ 2 . Alternatively, at fixed SZE signal, there is a scatter of a factor of ~ 2 in estimated virial mass. Unless the observational uncertainties are significantly underestimated, the data show substantial intrinsic scatter. Moreover, this scatter is comparable to the range of our sample and, therefore, the error on the slope derived from our least-squares fit to the data is likely to be underestimated (see Andreon & Hurn 2010, for a detailed discussion of a Bayesian approach to fitting relations with measurement uncertainties and intrinsic scatter in both quantities).

TABLE 1
HECS DYNAMICAL MASSES AND SZE SIGNALS

Cluster	z	σ_p	$M_{100,v}$	$M_{100,c}$	$Y_{SZ}D_A^2$ (350 kpc)	$Y_{SZ}D_A^2$ (r_{2500})	SZE
		km s $^{-1}$	$10^{14} M_\odot$	$10^{14} M_\odot$	10^{-5}Mpc^{-2}	10^{-4}Mpc^2	Ref.
A267	0.2288	743^{+81}_{-61}	6.86 ± 0.82	4.26 ± 0.14	3.08 ± 0.34	0.42 ± 0.06	1
A697	0.2812	784^{+77}_{-59}	6.11 ± 0.69	5.96 ± 3.51	—	1.29 ± 0.15	1
A773	0.2174	1066^{+77}_{-63}	18.4 ± 1.7	16.3 ± 0.7	5.40 ± 0.57	0.90 ± 0.10	1
Zw2701	0.2160	564^{+63}_{-47}	3.47 ± 0.42	2.69 ± 0.30	1.46 ± 0.016	0.17 ± 0.02^a	2
Zw3146	0.2895	752^{+92}_{-67}	6.87 ± 0.89	4.96 ± 0.91	—	0.71 ± 0.09	1
A1413	0.1419	674^{+81}_{-60}	6.60 ± 0.85	3.49 ± 0.15	3.47 ± 0.24	0.81 ± 0.12	1
A1689	0.1844	886^{+63}_{-52}	15.3 ± 1.4	9.44 ± 5.66	7.51 ± 0.60	1.50 ± 0.14	1
A1763	0.2315	1042^{+79}_{-64}	16.9 ± 1.6	12.6 ± 1.5	3.10 ± 0.32	0.46 ± 0.05^a	2
A1835	0.2507	1046^{+66}_{-55}	19.6 ± 1.6	20.6 ± 0.3	6.82 ± 0.48	1.37 ± 0.11	1
A1914	0.1659	698^{+46}_{-38}	6.70 ± 0.57	6.21 ± 0.21	—	1.08 ± 0.09	1
A2111	0.2290	661^{+57}_{-45}	4.01 ± 0.41	4.77 ± 1.23	—	0.55 ± 0.12	1
A2219	0.2256	915^{+53}_{-45}	12.8 ± 1.0	12.0 ± 4.7	6.27 ± 0.26	1.19 ± 0.05^a	2
A2259	0.1606	735^{+67}_{-53}	5.59 ± 0.60	4.90 ± 1.69	—	0.27 ± 0.10	1
A2261	0.2249	725^{+75}_{-57}	7.13 ± 0.83	5.10 ± 2.07	—	0.71 ± 0.09	1
RXJ2129	0.2338	684^{+88}_{-64}	4.31 ± 0.57	2.94 ± 0.13	—	0.40 ± 0.07	1

NOTE. — ^aExtrapolated to r_{2500} using the best-fit relation between $Y_{SZ}D_A^2$ (350kpc) and $Y_{SZ}D_A^2(r_{2500})$ for eight clusters in common between B08 and M09.

NOTE. — Redshift z and velocity dispersion σ_p are computed for galaxies defined as members using the caustics. Masses $M_{100,v}$ and $M_{100,c}$ are evaluated using the virial mass profile and caustic mass profile respectively.

NOTE. — REFERENCES: SZE data are from (1) Bonamente et al. 2008 and (2) Marrone et al. 2009.

Our shallow slopes may also arise in part from the fact that our sample, which has been assembled from the literature and whose selection function is difficult to determine, is likely to be biased against clusters with small mass and low SZE signal. Larger samples should determine whether unknown observational biases or issues in the physical understanding of the relation account for this discrepancy.

4. DISCUSSION

The strong correlation between masses from galaxy dynamics and SZE signals indicates that the SZE is a reasonable proxy for cluster mass. B08 compare SZE signals to X-ray observables, in particular the temperature T_X of the intracluster medium and $Y_X = M_{gas}T_X$, where M_{gas} is the mass of the ICM (see also Plagge et al. 2010). Both of these quantities are measured within r_{500} , a significantly smaller radius than r_{100} where we measure virial mass. M09 compare SZE signals to masses estimated from gravitational lensing measurements. The lensing masses are measured within a radius of 350 kpc. For the clusters studied here, this radius is smaller than r_{2500} and much smaller than r_{100} . Numerical simulations indicate that the scatter in masses measured within an over-density δ decreases as δ decreases (White 2002), largely because variations in cluster cores are averaged out at larger radii. Thus, the dynamical measurement reaching to larger radius may provide a more robust indication of the relationship between the SZE measurements and cluster mass.

The $Y_{SZ}D_A^2 - M_{lens}$ data presented in M09 show a weaker correlation than our optical dynamical properties. A Spearman test rejects the hypothesis of uncorrelated data for the M09 data at only the 94.8% confidence level, compared to the 98.4–99.8% confidence levels for our optical dynamical properties. One possibility is that M_{lens}

is more strongly affected by substructure in cluster cores and by line-of-sight structures than are the virial masses and velocity dispersions we derive.

Few measurements of SZE at large radii ($> r_{500}$) are currently available. Hopefully, future SZ data will allow a comparison between virial mass and Y_{SZ} within similar apertures.

5. CONCLUSIONS

Our first direct comparison of virial masses, velocity dispersions, and SZ measurements for a sizable cluster sample demonstrates a strong correlation between these observables (98.4–99.8% confidence). The SZE signal increases with cluster mass. However, the slopes of both the $Y_{SZ} - \sigma$ relation ($Y_{SZ} \propto \sigma_p^{2.94 \pm 0.74}$) and the $Y_{SZ} - M_{100}$ relation ($Y_{SZ} \propto M_{100}^{1.11 \pm 0.16}$) are significantly shallower (given the formal uncertainties) than the slopes predicted by numerical simulations (4.76 and 1.60 respectively).

This result may be partly explained by a bias against less massive clusters that could artificially flatten our measured slopes. Unfortunately, the selection function of our sample is unknown and we are unable to quantify the size of this effect. More importantly, our sample indicates that the relation between SZE and virial mass estimates (or velocity dispersion) has a non-negligible intrinsic scatter. A complete, representative cluster sample is required to robustly determine the size of this scatter, its origin, and its possible effect on the SZE as a mass proxy.

Curiously, Y_{SZ} is more strongly correlated with both σ_p and M_{100} than with M_{lens} (M09). Comparison of lensing masses and cluster velocity dispersions (and virial masses) for larger, complete, objectively selected samples of clusters may resolve these differences.

The full HeCS sample of 53 clusters will provide a large

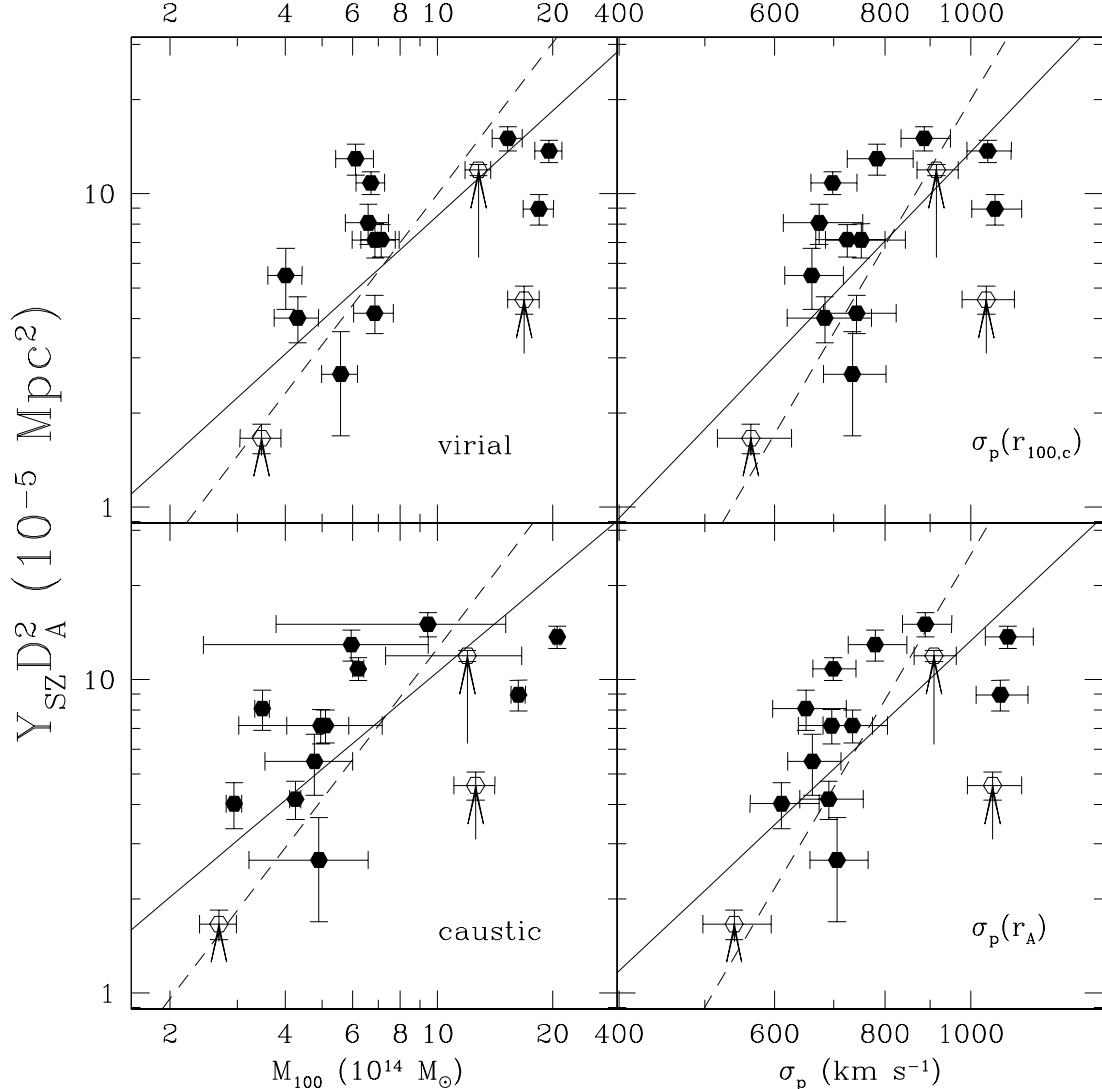


FIG. 2.— Integrated S-Z Compton parameter $Y_{SZ}D_A^2$ versus dynamical properties for 15 clusters from HeCS. *Left panels:* SZE data versus virial mass M_{100} estimated from the virial mass profile (top) and the caustic mass profile (bottom). Solid and open points indicate SZ measurements from B08 and M09 respectively. The dashed line shows the slope of the scaling predicted from numerical simulations: $Y_{SZ} \propto M^{1.6}$ (Motl et al. 2005), while the solid line shows the ordinary least-squares bisector. Arrows show the aperture corrections to the SZE measurements (see text). *Right panels:* SZE data versus projected velocity dispersions measured for galaxies inside the caustics and (top) inside $r_{100,c}$ estimated from the caustic mass profile and (bottom) inside the Abell radius 2.14 Mpc. The dashed line shows the scaling predicted from simulations: $Y_{SZ} \propto M^{1.6}$ (Motl et al. 2005) and $\sigma \propto M^{0.33}$ (Evrard et al. 2008). The solid line shows the ordinary least-squares bisector. Data points and arrows are defined as in the left panels.

sample of clusters with robustly measured velocity dispersions and virial masses as a partial foundation for these comparisons.

We thank Stefano Andreon for fruitful discussions about fitting scaling relations with measurement errors

and intrinsic scatter in both quantities. AD gratefully acknowledges partial support from INFN grant PD51. We thank Susan Tokarz for reducing the spectroscopic data and Perry Berlind and Mike Calkins for assisting with the observations.

Facilities: MMT (Hectospec)

REFERENCES

- Adelman-McCarthy, J. K. et al. 2008, ApJS, 175, 297
- Andreon, S. & Hurn, M. A. 2010, MNRAS in press, arXiv:1001.4639
- Böhringer, H. et al. 2004, A&A, 425, 367
- Biviano, A. & Girardi, M. 2003, ApJ, 585, 205
- Bonamente, M., Joy, M., LaRoque, S. J., Carlstrom, J. E., Nagai, D., & Marrone, D. P. 2008, ApJ, 675, 106
- Carlstrom, J. et al. 2010, ArXiv e-prints
- Danese, L., de Zotti, G., & di Tullio, G. 1980, A&A, 82, 322
- Diaferio, A. 1999, MNRAS, 309, 610
- . 2009, ArXiv e-prints
- Diaferio, A., Geller, M. J., & Rines, K. J. 2005, ApJ, 628, L97
- Ebeling, H., Edge, A. C., Allen, S. W., Crawford, C. S., Fabian, A. C., & Huchra, J. P. 1998, MNRAS, 301, 881

- Evrard, A. E. et al. 2008, ApJ, 672, 122
 Fabricant, D., Lecar, M., & Gorenstein, P. 1980, ApJ, 241, 552
 Fabricant, D. et al. 2005, PASP, 117, 1411
 Henry, J. P., Evrard, A. E., Hoekstra, H., Babul, A., & Mahdavi, A. 2009, ApJ, 691, 1307
 Hincks, A. D. et al. 2009, ArXiv e-prints
 Kravtsov, A. V., Vikhlinin, A., & Nagai, D. 2006, ApJ, 650, 128
 Lau, E. T., Nagai, D. & Kravtsov, A. V. 2010, ApJ, 708, 1419
 Locutus Huang, C. et al. 2009, ArXiv e-prints
 Lopes, P. A. A., de Carvalho, R. R., Kohl-Moreira, J. L., & Jones, C. 2009, ArXiv e-prints
 Majumdar, S. & Mohr, J. J. 2004, ApJ, 613, 41
 Mantz, A., Allen, S. W., Ebeling, H., & Rapetti, D. 2008, MNRAS, 387, 1179
 Mantz, A., Allen, S. W., Ebeling, H., Rapetti, D., & Drlica-Wagner, A. 2009, ArXiv e-prints
 Marrone, D. P. et al. 2009, ApJ, 701, L114
 Motl, P. M., Hallman, E. J., Burns, J. O., & Norman, M. L. 2005, ApJ, 623, L63
 Muchovej, S. et al. 2007, ApJ, 663, 708
 Nagai, D., Vikhlinin, A., & Kravtsov, A. V. 2007, ApJ, 655, 98
 Plagge, T. et al. 2010, ArXiv e-prints
 Richard, J. et al. 2010, ArXiv e-prints
 Rines, K. & Diaferio, A. 2006, AJ, 132, 1275
 Rines, K., Diaferio, A., & Natarajan, P. 2007, ApJ, 657, 183
 —, 2008, ApJ, 679, L1
 Rines, K., Geller, M. J., Kurtz, M. J., & Diaferio, A. 2003, AJ, 126, 2152
 Rozo, E. et al. 2008, astro-ph/0703571
 Smith, G. P., Kneib, J., Smail, I., Mazzotta, P., Ebeling, H., & Czoske, O. 2005, MNRAS, 359, 417
 Staniszewski, Z. et al. 2009, ApJ, 701, 32
 Sunyaev, R. A. & Zeldovich, Y. B. 1972, Comments on Astrophysics and Space Physics, 4, 173
 Vikhlinin, A. et al. 2009, ApJ, 692, 1060
 White, M. 2002, ApJS, 143, 241
 Zwicky, F. 1937, ApJ, 86, 217